The Astrophysical Journal, 995:8 (12pp), 2025 December 10 https://doi.org/10.3847/1538-4357/ae1463

Multiwavelength Observations of the Apparently Nonrepeating FRB 20250316A

Ye Li[1,34], Hui Sun[2,34], Lei Qian[2], Dong-Yue Li[2], Yan-Long Hua[1], Li-Ping Xin[2], Cheng-Kui Li[3], Yi-Han Wang[4,5,6], Jia-Rui Niu[2], Tian-Rui Sun[1], Zhu-Heng Yao[2], Jin-Jun Geng[1], Chi-Chuan Jin[2,7,8], Nanda Rea[9,10], Yuan Liu[2], Zhi-Chen Pan[2,11,12,13], Tao An[14], Vadim Burwitz[15], Zhi-Ming Cai[16], Jin-Huang Cao[2], Yong Chen[3], Hua-Qing Cheng[2], Wei-Wei Cui[3], Hua Feng[3], Peter Friedrich[15], Da-Wei Han[3], Jing-Wei Hu[2], Lei Hu[17,1], Yu-Xiang Huang[18,13], Shu-Mei Jia[3], Ji-An Jiang[19,20,21], Bin Li[1], Feng Li[22], Ming Liang[23], Yi-Fang Liang[1], Hao Liu[22], He-Yang Liu[2], Hua-Qiu Liu[16], Norbert Meidinger[15], Hai-Wu Pan[2], Arne Rau[15], Xin-Wen Shu[24], Chun Sun[2], Lian Tao[3], Jin-Long Tang[25], Zhen Wan[19,20], Hai-Ren Wang[1], Jian Wang[22,26], Jing Wang[2], Yun-Fei Xu[2], Yongquan Xue[19,20], Xuan Yang[1], Da-Zhi Yao[1], Yuhan Yao[27,28], Wen Zhao[19,20], Xiao-Fan Zhao[3], Hong-Fei Zhang[22], Jia-Heng Zhang[2], Juan Zhang[3], Mo Zhang[2], Song-Bo Zhang[1,29], Wen-Da Zhang[2], Xiao-Ling Zhang[1], Yong-He Zhang[16], Yong-Kun Zhang[2], Xian-Zhong Zheng[30], Yu-Hao Zhu[2], Ying-Xi Zuo[1], Sheng-Li Sun[31], Jian-Yan Wei[2,13], Wei-Wei Zhu[2,32], Peng Jiang[2,11,12,13], Weimin Yuan[2,13], Xue-Feng Wu[1], and Bing Zhang[33,5,6]

[1] Purple Mountain Observatory, Chinese Academy of Sciences, Nanjing 210023, People's Republic of China; yeli@pmo.ac.cn
[2] National Astronomical Observatories, Chinese Academy of Sciences, Beijing 100101, People's Republic of China; xlp@nao.cas.cn, zhuww@nao.cas.cn
[3] Key Laboratory of Particle Astrophysics, Institute of High Energy Physics, Chinese Academy of Sciences, Beijing 100049, People's Republic of China; lick@ihep.ac.cn
[4] Department of Astronomy, University of Wisconsin, Madison, WI 53706, USA
[5] Nevada Center for Astrophysics and Department of Physics and Astronomy, University of Nevada, Las Vegas, NV 89154, USA
[6] Department of Physics and Astronomy, University of Nevada, Las Vegas, NV 89154, USA
[7] School of Astronomy and Space Science, University of Chinese Academy of Sciences, Beijing 100049, People's Republic of China
[8] Institute for Frontier in Astronomy and Astrophysics, Beijing Normal University, Beijing 102206, People's Republic of China
[9] Institute of Space Sciences (ICE, CSIC), Campus UAB, Carrer de Can Magrans s/n, 08193, Barcelona, Spain
[10] Institut d'Estudis Espacials de Catalunya (IEEC), 08860, Castelldefels, Spain
[11] Guizhou Radio Astronomical Observatory, Guizhou University, Guiyang 550025, People's Republic of China
[12] Key Laboratory of Radio Astronomy and Technology (Chinese Academy of Sciences), A20 Datun Road, Chaoyang District, Beijing 100101, People's Republic of China
[13] School of Astronomy and Space Science, University of Chinese Academy of Sciences, Chinese Academy of Sciences, Beijing 100049, People's Republic of China
[14] Shanghai Astronomical Observatory, Chinese Academy of Sciences, Shanghai 200030, People's Republic of China
[15] Max-Planck-Institut fur extraterrestrische Physik, Giessenbachstrasse 1, 85748 Garching, Germany
[16] Innovation Academy for Microsatellites, Chinese Academy of Sciences, Shanghai 201210, People's Republic of China
[17] McWilliams Center for Cosmology, Department of Physics, Carnegie Mellon University, 5000 Forbes Avenue, Pittsburgh, PA 15213, USA
[18] Yunnan Observatories, Chinese Academy of Sciences, Kunming 650216, People's Republic of China
[19] Department of Astronomy, University of Science and Technology of China, Hefei 230026, People's Republic of China
[20] School of Astronomy and Space Sciences, University of Science and Technology of China, Hefei 230026, People's Republic of China
[21] National Astronomical Observatory of Japan, National Institutes of Natural Sciences, Tokyo 181-8588, Japan
[22] State Key Laboratory of Particle Detection and Electronics, University of Science and Technology of China, Hefei 230026, People's Republic of China
[23] National Optical Astronomy Observatory (NSF's National Optical-Infrared Astronomy Research Laboratory), 950 N Cherry Avenue, Tucson, AZ 85726, USA
[24] Department of Physics, Anhui Normal University, Wuhu, Anhui 241002, People's Republic of China
[25] Institute of Optics and Electronics, Chinese Academy of Sciences, Chengdu 610209, People's Republic of China
[26] Institute of Deep Space Sciences, Deep Space Exploration Laboratory, Hefei 230026, People's Republic of China
[27] Miller Institute for Basic Research in Science, 206B Stanley Hall, Berkeley, CA 94720, USA
[28] Department of Astronomy, University of California, Berkeley, CA 94720-3411, USA
[29] CSIRO Space and Astronomy, Australia Telescope National Facility, PO Box 76, Epping, NSW 1710, Australia
[30] Tsung-Dao Lee Institute and Key Laboratory for Particle Physics, Astrophysics and Cosmology, Ministry of Education, Shanghai Jiao Tong University, Shanghai, 201210, People's Republic of China
[31] Shanghai Institute of Technical Physics of the Chinese Academy of Sciences, People's Republic of China
[32] Institute for Frontiers in Astronomy and Astrophysics, Beijing Normal University, Beijing 102206, People's Republic of China
[33] Department of Physics, University of Hong Kong, Pokfulam Road, Hong Kong, People's Republic of China
Received 2025 August 18; revised 2025 September 19; accepted 2025 October 10; published 2025 December 2

Abstract

The physical origin of fast radio bursts (FRBs) remains uncertain. Although multiwavelength observations have been widely conducted, only Galactic FRB 20200428D is associated with an X-ray burst from the magnetar SGR J1935+2154. Here we present multiwavelength follow-up observations of the nearby bright FRB 20250316A, including the Five-hundred-meter Aperture Spherical radio Telescope (FAST), Einstein Probe (EP) X-ray mission, Chandra X-ray Observatory, Wide Field Survey Telescope (WFST), and Space Variable Objects Monitor/Visible Telescope (SVOM/VT). The 13.08 hr FAST follow-up campaign without pulse detection

[34] These authors contributed equally.

requires an energy distribution flatter than those of well-known repeating FRBs, suggesting that this burst is likely a one-off event. A prompt EP follow-up and multiepoch observational campaign totaling >100 ks led to the detection of an X-ray source within the angular resolution of its Follow-up X-ray Telescope (FXT; 10″). A subsequent Chandra observation revealed this source to be offset by 7″ from the FRB position and established a 0.5–10 keV flux upper limit of 7.6×10^{-15} erg cm^{-2} s^{-1} at the FRB position, corresponding to $\sim 10^{39}$ erg s^{-1} at the 40 Mpc distance of the host galaxy NGC 4141. These results set one of the most stringent limits on X-ray emission from a nonrepeating FRB, disfavoring ultraluminous X-ray sources as counterparts of apparently one-off FRBs and offering critical insights into afterglow models. Our study suggests that an arcsecond localization of both the FRB and its potential X-ray counterpart is essential for exploring the X-ray counterpart of an FRB.

Unified Astronomy Thesaurus concepts: Radio transient sources (2008); Radio bursts (1339); Transient sources (1851)

Materials only available in the online version of record: machine-readable table

1. Introduction

Fast radio bursts (FRBs) are millisecond-duration extragalactic radio transients (D. R. Lorimer et al. 2007). Among the nearly 1000 known FRB sources, fewer than 10% exhibit repeating bursts (L. G. Spitler et al. 2016; CHIME/FRB Collaboration et al. 2021, 2023). Although their origin remains unclear, the association between FRB 20200428D and a pair of X-ray pulses from the Milky Way magnetar SGR 1935+2154 (S. Mereghetti et al. 2020; CHIME/FRB Collaboration et al. 2020; C. K. Li et al. 2021) reveals that at least low-luminosity FRBs can be produced by magnetars.

While multiwavelength counterparts of typical extragalactic FRBs have been searched for, no conclusive association has been established (see B. Zhang 2024 for a review). The campaigns include well-studied repeating sources, such as FRB 20121102A (P. Scholz et al. 2016), FRB 20180301A (S. Laha et al. 2022), FRB 20180916B (M. Pilia et al. 2020; P. Scholz et al. 2020), FRB 20190520B (J. Sydnor et al. 2025), FRB 20220912A (A. M. Cook et al. 2024), and FRB 20240114A (F. Eppel et al. 2025). The most stringent limits in X-ray luminosity come from the nearby (3.6 Mpc) repeating FRB 20200120E (A. B. Pearlman et al. 2025), which exclude X-ray counterparts similar to ultraluminous X-ray sources (ULXs) or the Crab Nebula. However, most bursts from FRB 20200120E are fainter than typical FRBs (M. Bhardwaj et al. 2021; F. Kirsten et al. 2022; B. Zhang 2024), and its multiwavelength signals may also differ from those of typical FRBs. For apparently nonrepeating FRBs, constraints are usually much looser, because they rely primarily on telescopes with large fields of view (FOVs) and relatively poor sensitivities, such as AGILE (F. Verrecchia et al. 2021), Konus-Wind (A. Ridnaia et al. 2024), AstroSat-CZTI (G. Waratkar et al. 2025), and Fermi (G. Principe et al. 2023). Although two apparently nonrepeating FRBs, FRB 20190608B and FRB 20200430A, constrain X-ray luminosities to be $<10^{40}$ erg s^{-1}, the observations occurred nearly 2 yr after the bursts, and both sources are distant, with redshifts >0.1 (T. Eftekhari et al. 2023).

FRB 20250316A was detected by the Canadian Hydrogen Intensity Mapping Experiment (CHIME; M. Ng & CHIME/FRB Collaboration 2025; CHIME/FRB Collaboration et al. 2025) at 08:33:50.859038 (3) UTC on 2025 March 16 (topocentric at 400 MHz). The burst is very bright, with a peak flux of 1.2 ± 0.1 kJy and a fluence of 1.7 ± 0.2 kJy ms. High-cadence radio follow-up radio observations detected no pulse (O. S. Ould-Boukattine et al. 2025; CHIME/FRB Collaboration et al. 2025). The initial localization has arcminute uncertainties. Subsequent localization using the CHIME core and its three outriggers refined the position to (R.A., decl.) = ($12^{\rm h}09^{\rm m}44\overset{\rm s}{.}319$, $+58^{\rm d}50^{\rm m}56\overset{\rm s}{.}708$), with 1σ positional uncertainties of 68 mas (semimajor axis) and 57 mas (semiminor axis) at a position angle of $-0\overset{\circ}{.}26$ east of north (S. Andrew & Chime/FRB Collaboration 2025; CHIME/FRB Collaboration et al. 2025). This FRB is positionally associated with the nearby spiral galaxy NGC 4141, at a distance of 37–44 Mpc based on the Tully–Fisher relation (J. G. Sorce et al. 2014; R. B. Tully et al. 2016). While an infrared counterpart candidate from James Webb Space Telescope observations was reported (P. K. Blanchard et al. 2025), no clear optical counterpart was detected in MMT and Gemini observations (CHIME/FRB Collaboration et al. 2025). Assuming a host galaxy distance of 40 Mpc and a central frequency of 600 MHz for CHIME, the isotropic energy and luminosity of the FRB are $(2.0 \pm 0.2) \times 10^{39}$ erg and $(1.4 \pm 0.1) \times 10^{42}$ erg s^{-1}, respectively.

Due to its proximity and brightness, FRB 20250316A provides an excellent opportunity for multiwavelength counterpart searches and repeatability studies. To achieve this, we conducted radio, X-ray, and optical follow-up observations shortly after its discovery was reported. The structure of this paper is as follows: Section 2 describes the observations, and Section 3 presents the data analysis and results. We discuss the physical implications in Section 4, and we conclude with a summary in Section 5.

2. Observations

This section summarizes our multiwavelength observations of FRB 20250316A in radio, X-ray, and optical bands. The timeline relative to the FRB is shown in Figure 1.

2.1. Radio Observations

Following the report of FRB 20250316A (M. Ng & CHIME/FRB Collaboration 2025), we triggered the Five-hundred-meter Aperture Spherical radio Telescope (FAST) for follow-up monitoring. Eight sessions between 2025 March 17 and 24 were conducted as part of FAST Director Discretion Time and the FAST FRB key science project (L. Qian et al. 2025) in tracking mode. Data from all 19 beams of the FAST *L*-band receiver (1.05–1.45 GHz) were channelized into 4096 frequency channels, sampled at 49.153 μs, and recorded in PSRFITS search mode with dual linear polarization signals 8 bit sampled and processed using ROACH 2. A 1 K noise-switched calibration signal was taken before each observation. The total exposure time was 13.08 hr (13 hr and 5 minutes) across all sessions (Table 1).

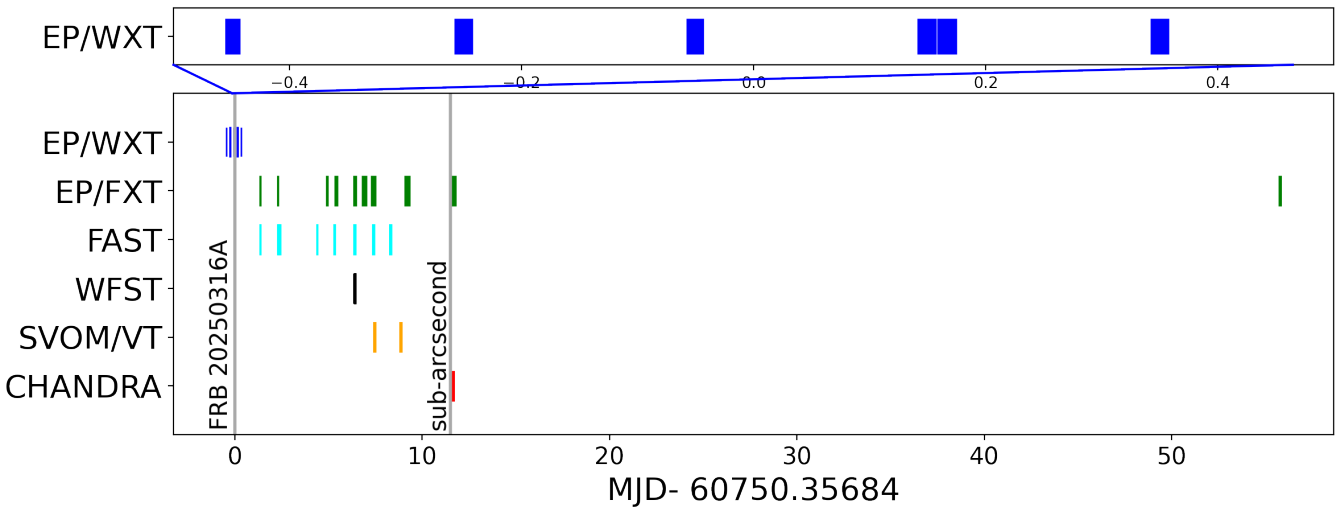

Figure 1. The timeline of the FRB 20250316A follow-up observations. For EP/WXT, only those observations within 12 hr before and after the FRB are presented. Vertical gray lines indicate the time of FRB 20250316A and the time at which FRB 20250316A was localized to be arcsecond accuracy.

2.2. X-Ray Observations

2.2.1. Einstein Probe

The Einstein Probe (EP; W. Yuan et al. 2022) is an X-ray mission launched in 2024 January. It carries two instruments: the Wide-field X-ray Telescope (WXT), a monitoring instrument with an FOV of 3600 deg^2, and the Follow-up X-ray Telescope (FXT), which provides a large effective area and an angular resolution of $\sim 10''$. WXT covered the position of FRB 20250316A in the survey mode six times within a 24 hr window centered on the burst, with a total exposure of 2 hr (Figure 1 and Table 2). However, the FRB position was not covered at the burst time. The temporally closest observation started on 2025 March 16 at 07:11:07 UTC and ended at 07:30:49 UTC, about 1 hr before the burst. This was followed by the first post-burst observation, starting on 2025 March 16 at 11:57:59 UTC, about 3.5 hr after the burst, with an exposure time of 1324 s.

Following the discovery of FRB 20250316A, we observed the FRB field using the FXT (Y. Chen et al. 2021) on board EP. Our campaign consisted of 10 target-of-opportunity observations: nine were taken between 32 hr and 11 days post-burst (Figure 1 and Table 2). An additional late-time observation was carried out on 2025 May 11 to investigate the variability of a previously reported X-ray source in the field, EP J120944.2+585060 (H. Sun et al. 2025a, 2025b).

2.2.2. Chandra

We conducted a follow-up observation of the FRB 20250316A field with the High Resolution Camera (HRC) on the Chandra X-ray Observatory, aiming to search for a potential X-ray counterpart and obtain an arcsecond localization of EP J120944.2+585060. The observation started on 2025 March 27 at 21:31:27 UTC, with an exposure of 10.89 ks, under a Director's Discretionary Time (DDT) proposal (PI: Sun, Chandra ObsId 30871). The target coordinate was (R.A., decl.) (J2000) = (12:09:41.52, +58:50:30.14), the position of EP J120944.2+585060. We selected HRC owing to the soft spectrum of EP J120944.2+585060 and its superior effective area below 1 keV compared to other Chandra instruments. The HRC's subarcsecond resolution provides an order-of-magnitude improvement in positional accuracy over the EP-FXT.

Table 1
FAST Observations

Start Time (UTC)	MJD	Exposure (s)	Upper Limits[a] (mJy ms)
2025-03-17 16:45:00	60751.69792	3600	15.3
2025-03-18 15:38:00	60752.65139	3600	15.3
2025-03-18 16:50:00	60752.70139	7200	15.3
2025-03-20 17:28:00	60754.72778	3900	15.3
2025-03-21 15:39:00	60755.65208	3900	15.3
2025-03-22 16:56:00	60756.70556	7200	15.3
2025-03-23 17:00:00	60757.70833	7200	15.3
2025-03-24 14:58:00	60758.62361	7200	15.3

Note.
[a] A burst width of 1 ms was assumed. Signal-to-noise ratio > 7.

2.3. Optical Observations

2.3.1. WFST

The Wide Field Survey Telescope (WFST) is a 2.5 m aperture facility located in Lenghu, China (T. Wang et al. 2023). It features a 6.5 deg^2 FOV enabled by its optical design and a mosaic CCD camera. On 2025 March 22, we carried out 21 r-band exposures of the FRB 20250316A field, 180 s each, yielding a total integration time of 63 minutes. The start times, exposure durations, and filters of these observations are listed in Tables 3 and A1.

2.3.2. SVOM/VT

The Space Variable Objects Monitor (SVOM) is a China–France mission designed to detect gamma-ray bursts (J. Wei et al. 2016). In addition to gamma-ray instruments—GRM (gamma rays), ECLAIR (hard X-rays), and MXT (soft X-rays)—SVOM carries a 43 cm Visible Telescope (VT) with a dichroic beam splitter dividing light into two channels: VT_B (0.4–0.65 μm) and VT_R (0.65–1 μm). SVOM/VT conducted two runs of observations targeting FRB 20250316A,

Table 2
X-Ray Observations

Telescope	Start Time (UTC)	ObsID	Exposure Time (s)	Flux (erg cm^{-2} s^{-1})[a]	
				EP J120944.2+585060	FRB 20250316A
EP-WXT	2025-03-16 07:11:07	11916648071	1182	⋯	$<1.1 \times 10^{-11}$
EP-WXT	2025-03-16 11:57:59	11916648077	1324	⋯	$<7.2 \times 10^{-12}$
EP-FXT	2025-03-17 16:57:29	08500000303	2994	⋯	$<3.4 \times 10^{-14}$
EP-FXT	2025-03-18 15:22:38	08500000304	2982	$3.4^{+1.0}_{-0.9} \times 10^{-14}$	⋯
EP-FXT	2025-03-21 05:50:01	08500000311	5804	$2.9^{+0.7}_{-0.6} \times 10^{-14}$	⋯
EP-FXT	2025-03-21 17:02:17	08500000317	10850	$1.6^{+0.4}_{-0.4} \times 10^{-14}$	⋯
EP-FXT	2025-03-22 17:03:26	08500000319	10480	$2.3^{+0.5}_{-0.4} \times 10^{-14}$	⋯
EP-FXT	2025-03-23 04:15:56	08500000320	16970	$2.2^{+0.4}_{-0.3} \times 10^{-14}$	⋯
EP-FXT	2025-03-23 15:28:24	08500000321	19558	$2.4^{+0.3}_{-0.3} \times 10^{-14}$	⋯
EP-FXT	2025-03-25 10:41:53	08500000325	21823	$1.9^{+0.3}_{-0.3} \times 10^{-14}$	⋯
EP-FXT	2025-03-27 22:14:34	08500000326	19607	$2.5^{+0.4}_{-0.4} \times 10^{-14}$	⋯
EP-FXT	2025-05-11 02:36:50	06800000592	7391	$2.2^{+0.6}_{-0.5} \times 10^{-14}$	⋯
Chandra/HRC	2025-03-27 21:32:27	30871	10890	$1.6^{+0.5}_{-0.3} \times 10^{-14}$	$<7.6 \times 10^{-15}$

Note.
[a] The unabsorbed X-ray fluxes are given as 90% upper limits for nondetections at the position of FRB 20250316A. For sources detected within the instrument's positional uncertainty, we report the measured fluxes with their 1σ statistical uncertainties.

Table 3
Optical Observations and Upper Limits

Start Time	MJD	T_{exp} (s)	Band	mag_{lim}
WFST				
Single images				
2025-03-22 17:04:19	60756.71133	180(21)	r	22.94–23.34
Stacked images		180*21	r	24.18
SVOM/VT				
Single images				
2025-03-23 18:22:00	60757.76458	60(101)	VT_B	21.90–22.10
		60(101)	VT_R	21.76–22.00
2025-03-25 04:22:05	60759.18131	60(97)	VT_B	⋯
		60(97)	VT_R	⋯
Stacked images		60*101	VT_B	24.17
		60*101	VT_R	24.04

simultaneously acquiring VT_B and VT_R data. The first run began on 2025 March 23 18:22:00 UTC, the second on 2025 March 25 04:22:05 UTC. Each exposure was 60 s. After removing images affected by background noise or distorted point-spread functions, 101 and 97 good-quality frames were obtained in the two runs for each band. Details are listed in Tables 3 and A1.

3. Data Analysis and Results

3.1. Radio

Single pulses were searched for in the FAST data using PRESTO (S. M. Ransom 2001; S. M. Ransom et al. 2002, 2003), with a dispersion measure range of 140–180 pc cm^{-3} and a step size of 0.1 pc cm^{-3}. No pulses with signal-to-noise ratio > 7 were detected, which corresponds to a fluence threshold of $\sim$15.3 mJy ms for a fiducial burst width of 1 ms and a bandwidth of 400 MHz (Table 1). This fluence limit translates to an energy upper limit of 1.5×10^{34} erg, assuming a source distance of 40 Mpc.

3.2. X-Ray

3.2.1. Einstein Probe

Using the WXT data reduction pipeline and calibration database (CALDB; H. Cheng et al. 2025), we analyzed the observations obtained 1.5 hr before and 3.5 hr after FRB 20250316A. No significant X-ray sources (above a 5σ significance threshold) were detected within the positional uncertainty radius ($\leqslant 3'$) centered at the FRB location (Figure 2, top left panel). For these two observations, we extracted the source counts from a circular region with a radius of $9'$ at the FRB position, enclosing over 90% of the photons within the focal spot region as determined by the WXT ground calibration, and the background counts from an annulus with inner and outer radii of $18'$ and $36'$, respectively, as shown in Figure 2. We derived the 90% confidence count rate upper limits of 0.0057 and 0.0036 counts s^{-1}, respectively, in the 0.5–4 keV range. Assuming an absorbed power-law spectrum with a photon index of 2 and a Galactic absorption column density of $N_H = 1.4 \times 10^{20}$ cm^{-2}, the flux limits are 1.1×10^{-11} erg cm^{-2} s^{-1} and 7.2×10^{-12} erg cm^{-2} s^{-1}, respectively, corresponding to 2.1×10^{42} erg s^{-1} and 1.4×10^{42} erg s^{-1} assuming a luminosity distance of 40 Mpc.

In the first FXT observation, which began at 2025-03-17T16:57:29 with an exposure time of 2.9 ks, no X-ray sources were detected within the CHIME error region. In the second observation, starting at 2025-03-18T15:23:50 with the same exposure time of 2.9 ks, FXT detected a weak, uncatalogued X-ray source, designated as EP J120944.2+585060. The position of this source is generally consistent with the first refined localization provided by CHIME (C. Leung & Chime/Frb Collaboration 2025). The source was observed in all eight subsequent FXT observations. For each observation, we extracted the source using a circular region with a $1'$ radius. The background was selected from an annulus with inner and outer radii of $1'$ and $3'$, respectively, where we excluded

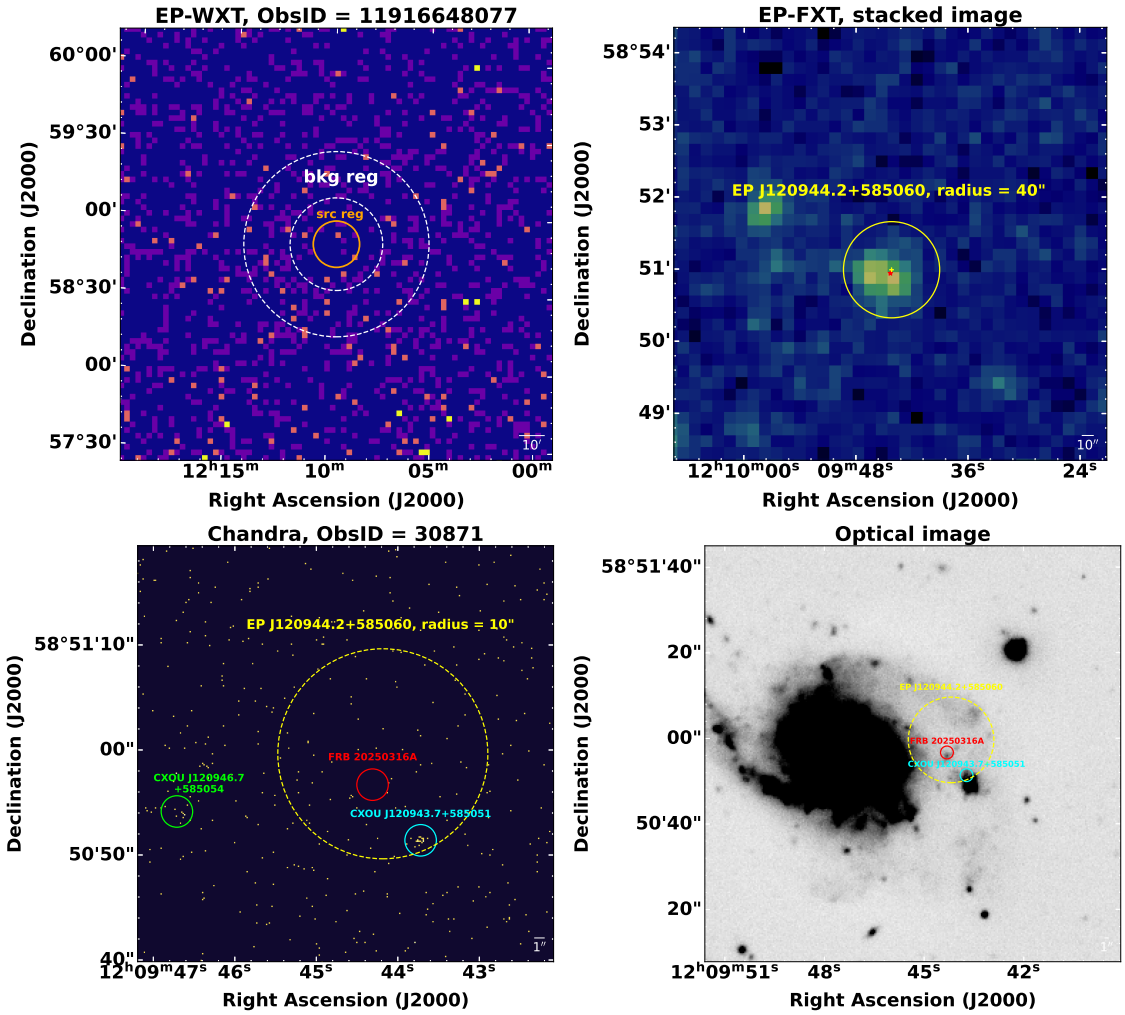

Figure 2. X-ray and optical images of the FRB 20250316A field. Top left: the EP-WXT image obtained from the observation 3.5 hr after the FRB, with the source and background regions marked for upper-limit analysis. Top right: the stacked image from all FXT observations, with a yellow circle centered on the position initially reported from the early detection. The red star marks the position of FRB 20250316A. Bottom left: Chandra image. An X-ray source CXOU J120943.7 +585051 (cyan) offset by $\sim 7''$ from the FRB position (red circle; projected distance: 1.36 kpc) is located within the error circle of EP J120944.2+585060 (yellow), along with one faint Chandra object (green) at a separation of $\sim 22''$ from the first. Bottom right: WFST image. Both FRB 20250316A (red) and CXOU J120943.7 +585051 (cyan) reside in separate extended regions.

contamination from bright sources. The FXT data were processed using the FXT data analysis software (fxtsoftware v1.20; http://epfxt.ihep.ac.cn/analysis). The process involved particle event identification, pulse invariant conversion, grade calculation and selection (grade 0–12), bad and hot pixel flag, and selection of good time intervals using housekeeping files.

The spectrum extracted from the stacked images of all the FXT observations (Figure 2, top right panel) was fitted in XSPEC (v12.14.1) with an absorbed power-law model. The best-fit photon index is 2.5 ± 0.2 (uncertainties at the 1σ confidence level), assuming the same Galactic absorption as previously introduced. When modeling the spectrum with the absorption as a free parameter, we found negligible intrinsic absorption. The photon index remains consistent with that obtained from the fixed-absorption fit.

The EP-FXT's angular resolution ($\sim 23''$ in half-power diameter; Y. Chen et al. 2025) and localization uncertainty ($\lesssim 10''$) are insufficient to conclusively associate the EP source with FRB 20250316A. Therefore, a Chandra/HRC observation was requested to investigate the potential association of the X-ray source with the FRB.

3.2.2. Chandra

We used the Chandra Interactive Analysis of Observations (CIAO, ver. 4.17; A. Fruscione et al. 2006) software package and the Chandra Calibration Database (CalDB, ver. 4.12) to reduce and analyze the Chandra observations. By applying the *vtpdetect* in CIAO for source detection, we identified an X-ray source (CXOU J120943.7+585051) within the FXT error circle (Figure 2, bottom left panel). The source is located at R. A. (J2000) = 12:09:43.72, decl. (J2000) = +58:50:51.4, with a positional uncertainty of $0.''74$ (68% confidence level, statistical + systematic). Employing a circular source region with a radius of $1''$ and a background annulus with inner and outer radii of $3''$ and $5''$, respectively, we obtained a detection significance of 8σ using the Li-Ma formula (T. P. Li & Y. Q. Ma 1983). The source count rate was derived using the *srcflux* tool, yielding a measurement of $1.56^{+0.44}_{-0.34} \times 10^{-3}$ counts s^{-1} (1σ uncertainties, 0.1–10.0 keV). Assuming an absorbed power-law model with a photon index $\Gamma = 2.5$ and a hydrogen column density $N_{\rm H} = 1.4 \times 10^{20}\,{\rm cm}^{-2}$, we estimated the unabsorbed 0.5–10 keV flux from the count rate using PIMMS (K. Mukai 1993) using the average spectral response

files provided within the tool. The resulting flux is $1.6^{+0.5}_{-0.3} \times 10^{-14}$ erg cm^{-2} s^{-1} (1σ uncertainties), generally consistent with previous EP-FXT measurements, thereby confirming this source as EP J120944.2+585060. The position of this source is offset by 7″ from the precise localization of FRB 20250316A provided by the full CHIME/FRB Outriggers (FRB Collaboration et al. 2025). The combined positional uncertainty for the two sources is approximately 0.″7 (derived from the subarcsecond uncertainties of both the FRB and Chandra/HRC positions), meaning that the observed spatial separation corresponds to nearly 10σ. This relatively large spatial separation suggests that EP J120944.2+585060 is not physically associated with FRB 20250316A.

We note the presence of another object, CXOU J120946.7+585054, detected at 4σ confidence level within 1′ of the FRB, at the coordinates of R.A. (J2000) = 12:09:46.71, decl. (J2000) = +58:50:54.1 (with a positional uncertainty of 0.″93, 68% confidence level, statistical + systematic; green circle in the bottom left panel of Figure 2). It is 22″ away from CXOU J120943.7+585051 and 20″ away from the nominal EP J120944.2+585060. It is difficult for FXT to resolve these two objects, as shown in the stacked FXT image (top right panel of Figure 2). The measured count rate for CXOU J120946.7+585054, obtained with *srcflux*, is $3.98^{+2.71}_{-1.65} \times 10^{-4}$ counts s^{-1} (1σ uncertainties, 0.1–10.0 keV). Assuming an absorbed power-law model with a photon index $\Gamma = 2$ and the galactic absorption, we estimated the unabsorbed 0.5–10 keV flux from the count rate using PIMMS to be $6.9^{+4.7}_{-2.9} \times 10^{-15}$ erg cm^{-2} s^{-1}. Thus, the fluxes of CXOU J120943.7+585051 measured from the FXT observations are contaminated by $\sim 30\%$ owing to CXOU J120946.7+585054. This contamination may explain why the FXT fluxes are slightly higher than the Chandra flux, although the difference is not statistically significant.

At the position of FRB 20250316A, we derive a 90% upper limit on the unabsorbed 0.5–10 keV flux of 7.6×10^{-15} erg cm^{-2} s^{-1}, assuming an absorbed power-law spectrum with a photon index of 2 and $N_{\rm H} = 1.4 \times 10^{20}$ cm^{-2}. For a distance of 40 Mpc from the host galaxy, this corresponds to a 0.5–10 keV X-ray luminosity upper limit of $\sim 10^{39}$ erg s^{-1}.

3.2.3. Properties of CXOU J120943.7+585051

Although the precise location of CXOU J120943.7+585051/EP J120944.2+585060 provided by Chandra rules out its association with FRB 20250316A, the nature of the X-ray source remains of interest. The source was detected by FXT in observations spanning over 50 days. The 0.5−10 keV light curve extracted at the Chandra position shows moderate variability (see Table 2 and Figure 3). However, a χ^2 test against a constant flux model yielded $\chi^2 = 8.15$ for 8 degrees of freedom, corresponding to a p-value of 0.419. This high p-value indicates that the observed data are consistent with the null hypothesis of no variability, showing no statistically significant deviation from a constant flux. Together, these results indicate that the flux remained stable within uncertainties across the earlier observations. The late-time observation in May further confirms this steady behavior.

With an estimated flux of 1.6×10^{-14} erg cm^{-2} s^{-1} inferred from the Chandra observation, this source, if associated with the host galaxy at 40 Mpc, corresponds to a luminosity of $\sim 3 \times 10^{39}$ erg s^{-1}. This places it within the typical luminosity range for ULXs, which are thought to be powered by accretion onto a compact object (a stellar-mass black hole, neutron star, or potentially an intermediate-mass black hole (IMBH)) at a luminosity comparable to or above the Eddington luminosity of stellar black holes (see P. Kaaret et al. 2017 for a review). Alternatively, if CXOU J120943.7+585051 is not associated with the FRB's host galaxy, it could be a foreground Galactic source (such as a cataclysmic variable) or a background extragalactic object like an active galactic nucleus (AGN). Distinguishing between these possibilities would require multiwavelength observations.

3.3. Optical

3.3.1. WFST

WFST images were reduced with standard optical procedures. After extracting objects using SExtractor (E. Bertin & S. Arnouts 1996), we cross-matched them with Gaia and refined the WCS using SCAMP (E. Bertin 2006). Photometric zero-points were calibrated with Pan-STARRS r-band magnitudes (K. C. Chambers et al. 2016). To examine host details, we stacked images using SWarp (E. Bertin et al. 2002) with median values. The stacked image is shown in the bottom right panel of Figure 2, with the positions of FRB 20250316A (red), EP J120944.2+585060 (yellow), and CXOU J120943.7+585051 (cyan) overplotted. FRB 20250316A and CXOU J120943.7+585051 lie in two extended regions, likely star-forming regions of the host galaxy. The center of the star-forming region hosting FRB 20250316A was determined at (R.A., decl.) = (182.°434782, 58.°848778) using the *centroid_com* function from Photutils. The FRB lies 1.″1 from this centroid (215 pc at 40 Mpc), consistent with CHIME/FRB Collaboration et al. (2025) and P. K. Blanchard et al. (2025). To assess systematic uncertainties, we also measured the offset between the FRB and the peak of the star-forming region, yielding 0.″8 (157 pc).

After this, we searched for possible transient optical counterparts of FRB 20250316A in individual images and the stacked image, using the DESI/Legacy Survey (DESI/LS)[35] r-band image as a template. Individual images were aligned to the DESI/LS stack with *reproject* (T. Robitaille et al. 2020) in Python and then subtracted using HOTPANTS (A. Becker 2015) with a kernel size of ∼1.5 times the WFST FWHM. No significant objects were found at the FRB 20250316A position in individual subtracted images. The upper limits were estimated as $\mathrm{mag_{lim}} = \mathrm{ZP} - 2.5\log_{10}(5\sigma\sqrt{2.226\,\mathrm{FWHM}})$, where ZP is the zero-point of each image and σ is the rms within 90″ of the FRB in the residual image. The 5σ upper limits are listed in Tables 3 and A1. An upper limit of 24.18 mag was estimated from the stacked image using a similar process, limited by the seeing and DESI/LS depth. This is generally consistent with the limits of the FRB optical counterpart from the MMT telescope ($r > 25$ mag on 2025 March 23) and Gemini ($g > 23.7$ mag on 2025 March 24; CHIME/FRB Collaboration et al. 2025).

3.3.2. SVOM/VT

We first stacked the images obtained on 2025 March 23 and 2025 March 25 individually, following the standard procedure using IRAF v2.16 (D. Tody 1986, 1993): (1) Images with abnormally high backgrounds or distorted stellar profiles were

[35] https://www.legacysurvey.org/

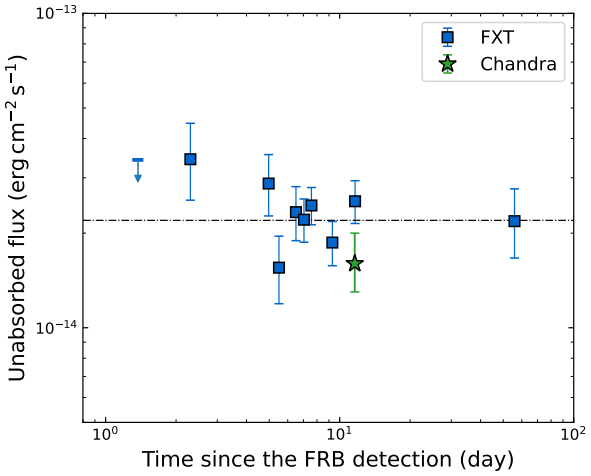

Figure 3. The X-ray light curve of EP J120944.2+585060/CXOU J120943.7 +585051 observed by EP-FXT (blue) and Chandra (green). Errors show 1σ statistical uncertainties. The dashed line shows the weighted mean flux derived from EP-FXT observations. The slightly higher flux measured by EP-FXT may be due to contamination from the nearby Chandra source.

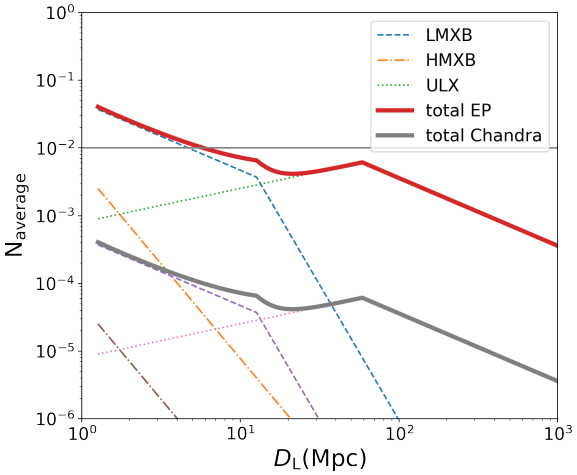

Figure 4. Averaged number of unrelated X-ray sources within the angular resolution for EP/FXT and Chandra telescope.

excluded. The remaining images underwent bias, dark, and flat-field corrections. (2) Precise astrometric alignment was performed with astrometry.net (D. Lang et al. 2010; P. Joseph & A. Dagore 2024) relative to a chosen reference frame using common bright stars. (3) The aligned images were then stacked with the IRAF.IMCOMBINE task with an average combination method, incorporating sigma-clipping to reject cosmic rays and bad pixels, improving the signal-to-noise ratio of the final stacked images. For both the VT_B and VT_R bands, we stacked 101 and 97 frames from 2025 March 23 and 2025 March 25, respectively, each with 60 s exposure. We then searched for possible optical counterparts with a similar process to that of WFST. Because SVOM/VT observations were taken on two different days and used custom-designed filters (400–650 nm for VT_B and 650–1000 nm for VT_R), we utilized the images from SVOM/VT itself as templates to perform image subtraction. Since signals temporally closer to the burst are expected to be more significant, the last single and the stacked images from 2025 March 25 were used as templates, for single and stacked image subtraction, respectively. The upper limits are summarized in Tables 3 and A1.

4. Physical Implications and Discussions

4.1. Probability of Chance Coincidence

The X-ray source CXOU J120943.7+585051 was detected by Chandra within the FXT error circle. Given its relatively large separation of 7″ from the FRB position, the source is unlikely to be physically associated with FRB 20250316A. To quantify the likelihood of such a chance alignment, we calculated the probability of chance coincidence in this section. It should be noted that alternative origins for CXOU J120943.7+585051, such as a foreground Galactic X-ray source or a background AGN, cannot be fully ruled out.

First, we estimate the probability of having an X-ray source within a circle with a 10″ radius on average. Based on the X-ray source density (A. Masini et al. 2020) at EP/FXT limiting flux, 10^{-14} erg cm^{-2} s^{-1} in 0.5–4 keV, the averaged number of X-ray sources within the EP/FXT angular resolution is 0.003.

Second, the density of X-ray sources within galaxies may be enhanced. Thus, we also calculated the probability of a random, unrelated ULX appearing within 10″ of the FRB position in a galaxy. A 10″ angular separation at 40 Mpc corresponds to a projected physical radius of 1.94 kpc. The likelihood of finding an unrelated ULX within this region depends critically on the host galaxy properties and the surface density of ULXs. For the general galaxy population, the average number of ULXs ($L_X > 10^{39}$ erg s^{-1}) is reported to be 0.88 ± 0.05 (K. Kovlakas et al. 2020). For a typical galactic disk of radius 15 kpc, the expected number of ULXs in a 1.94 kpc radius circle is $\sim(1.94/15)^2 \sim 0.016$, giving a 1.6% chance probability using a Poisson statistics. However, this probability is significantly enhanced in star-forming regions or star-forming galaxies, where ULXs are substantially more prevalent (H. Feng & R. Soria 2011; D. A. Swartz et al. 2011). In such active environments, the density of ULXs could be higher by a factor of 5–10, corresponding to a chance probability of approximately 8%–15% to detect an unrelated ULX-like source within 10″ in a star-forming galaxy.

In addition, for even nearby FRBs, low-mass X-ray binaries (LMXBs) and high-mass X-ray binaries (HMXBs) may contribute to contamination. Using a similar method to that above, and including the luminosity functions of LMXBs, HMXBs, and ULXs (S. Wang et al. 2016; M. Gilfanov et al. 2022), we estimate the average number of unrelated LMXBs, HMXBs, and ULXs expected within the angular resolution of EP/FXT (10″) and Chandra (1″) for different luminosity distances D_L, as shown in Figure 4. It shows that the chance of contamination from LMXBs, HMXBs, and ULXs is about 1% for EP/FXT and 0.01% for Chandra. Furthermore, given that around 20% of FRBs reside in host galaxies with AGN signals (T. Eftekhari et al. 2023; K. Sharma et al. 2024), the contamination from AGNs or IMBHs is then nonnegligible, especially for higher redshifts. These considerations highlight the importance of arcsecond-level localization for both FRBs and their potential X-ray counterparts, although EP/FXT candidates remain useful in most cases.

4.2. One-off or Repeating

One of the most critical questions in FRB research is whether all FRBs repeat. As a nearby FRB, FRB 20250316A

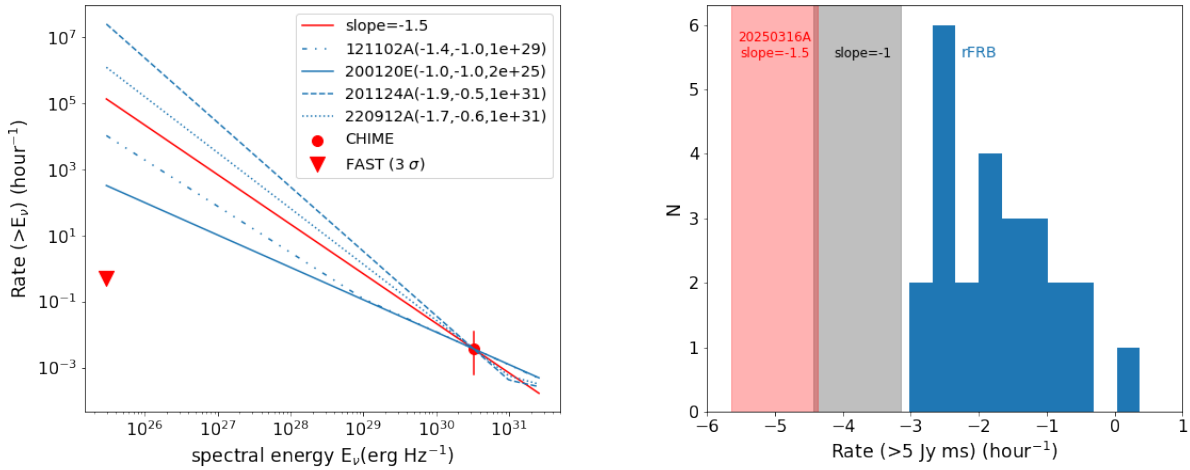

Figure 5. Left: CHIME FRB rate and the FAST 3σ upper limit compared with the spectral energy functions of repeating FRBs. A typical power law with a slope of -1.5 is plotted as a red solid line. The blue lines present the spectral energy functions of repeating FRBs, scaled to match the rate of FRB 20250316A at its spectral energy. Right: the FRB rate (>5 Jy ms) of FRB 20250316A estimated with multiple telescopes, assuming energy function slopes of -1.5 (red region) and -1.0 (gray region), compared with the CHIME-detected FRB rate (blue histogram).

provides a valuable opportunity to examine this issue. Observationally, it was detected by CHIME after 269.77 hr of exposures over 6 yr (CHIME/FRB Collaboration et al. 2025), corresponding to an FRB Poisson rate of 0.004 hr^{-1} with a 1σ range of 0.0006–0.012 hr^{-1} ($>1.7 \times 10^3$ Jy ms, corresponding to $>3.2 \times 10^{30}$ erg Hz^{-1}). FAST conducted 13.08 hr of follow-up observations over approximately 1 week (Section 3.1). Assuming a Poisson distribution, this indicates a 3σ upper limit of $<0.5\,\mathrm{hr}^{-1}$ (>15.5 mJy ms, corresponding to $>3.0 \times 10^{25}$ erg Hz^{-1}). The left panel of Figure 5 presents FRB rates estimated with CHIME (red circle) and the upper limit from FAST (red triangle). For comparison, we overplot the energy functions of repeating FRBs. The energy functions of repeating FRBs are empirically fitted as a power law, with a slope of ~ -1.5, spanning a range from -0.7 to -2.5 (C. J. Law et al. 2017; K. Gourdji et al. 2019). A flatter high-energy component has sometimes been proposed for repeating FRBs, such as FRB 20121102A (D. Li et al. 2021; D. M. Hewitt et al. 2022), FRB 20200120E (S. B. Zhang et al. 2024), FRB 20201124A (Y.-K. Zhang et al. 2022; F. Kirsten et al. 2024), and FRB 20220912A (O. S. Ould-Boukattine et al. 2025). Their energy functions are shown as blue lines, with the lower index, higher index, and break spectral energy labeled. The flatter component typically extends over 1–2 orders of magnitude in spectral energy. A comparison between FRB 20250316A and repeating FRBs reveals two possible scenarios. First, the typical power law with a slope of -1.5 (red solid line) predicts an FRB rate of $2.7 \times 10^5\,\mathrm{hr}^{-1}$ above the FAST limiting fluence of 15.5 mJy ms, more than five orders of magnitude larger than the FAST 3σ upper limit. Second, scaling the energy functions of repeating FRBs to the rate of FRB 20250316A at its spectral energy (blue lines) shows that repeating FRBs predict rates 3–7 orders of magnitude higher than the FAST upper limit.

We note that repeating FRBs are usually clustered, with waiting times often described by Weibull distributions (N. Oppermann et al. 2018; CHIME/FRB Collaboration et al. 2020; L. C. Oostrum et al. 2020; K. M. Rajwade et al. 2020; F. Kirsten et al. 2024). The Weibull shape parameter k characterizes clustering: bursts are clustered if $k < 1$, with typical values $k = 0.3$–0.9 (N. Oppermann et al. 2018; L. C. Oostrum et al. 2020; R. Luo et al. 2020). Using the simulation method of R. Luo et al. (2020), we obtained 3σ FRB rate upper limits of 2.0, 0.7, and 0.5 hr^{-1} (at FAST limiting fluence) for $k = 0.3$, 0.5, and 0.9, respectively, still 2–7 orders of magnitude below predictions from repeating FRB energy functions.

On the other hand, some repeating FRBs have $\leqslant 10$ bursts, with FRB rates of 10^{-3} to 2 bursts per hour at a completeness of 0.5–10 Jy ms (CHIME/FRB Collaboration et al. 2023). Their energy functions cannot be examined in detail. In order to compare with them, we estimated the FRB rate of FRB 20250316A by combining observations from multiple telescopes. A cumulative FRB rate with multiple telescopes can be estimated as

$$R(>E_\nu) = \frac{N}{\sum_i t_{\mathrm{obs},i} f(E_{\nu,i})/f(E_{\nu,0})},$$

where $f(E_\nu)$ is the energy function of FRBs, i iterates over different telescopes, and E_ν is the threshold of each telescope. To compare with the CHIME repeating FRBs, we adopt $f(E_{\nu,i}) \propto E_\nu^\alpha$ following CHIME/FRB Collaboration et al. (2023). Taking into account the observations of FAST, CHIME, and HyperFlash—a 25–32 m European radio telescope network that observed FRB 20250316A for 120 hr at L band with a limiting fluence of 15 Jy ms (O. S. Ould-Boukattine et al. 2025; CHIME/FRB Collaboration et al. 2025)—and assuming a slope of -1.5, we obtain a combined FRB 20250316A rate of $(1.3^{+3.0}_{-1.0}) \times 10^{-5}$ hr^{-1} (red region in the right panel of Figure 5). This region lies below all CHIME repeating FRBs (blue histogram). Using the flattest slope of well-studied repeating FRBs, ~ -1.0 (FRB 20200120E; S. B. Zhang et al. 2024), the rate is estimated to be $(2.2^{+5.0}_{-1.0}) \times 10^{-4}$ hr^{-1} (gray region), still below all CHIME repeating FRBs. Thus, FRB 20250316A is different from the currently known repeating FRB sample.

CHIME/FRB Collaboration et al. (2025) explored the repeatility of this burst by a simulation and concludes that the probability of detecting only one burst like FRB 20250316A in

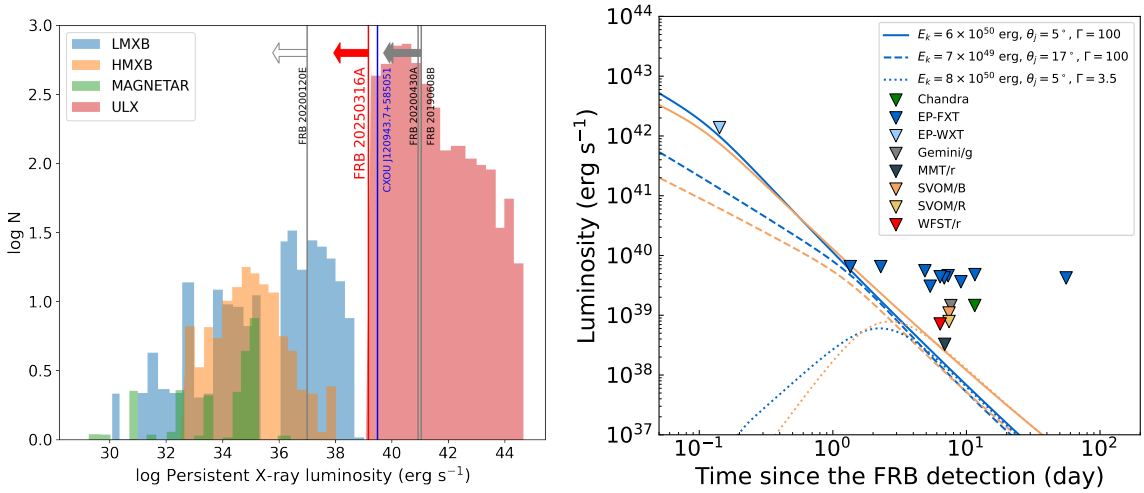

Figure 6. Left: upper limits on the persistent X-ray luminosity from the Chandra observation at the position of FRB 20250316A (red arrow). For comparison, the observed luminosities of LMXBs, HMXBs, magnetars, and ULXs are overplotted. Upper limits on the persistent X-ray luminosity from other one-off FRBs (filled arrows) and a repeating FRB (open arrow) are also shown. Right panel: multiwavelength constraints of FRB 20250316A. The predictions of afterglow models (Y. Wang et al. 2026) with different parameters are overplotted. Blue and orange lines are for X-ray and optical, respectively.

repeating FRBs is more significant than 5σ. With different methods, we have the same conclusion that FRB 20250316A is highly likely to be a one-off event. We caution, however, that this process assumes that the energy function of repeating FRBs is stable, whereas temporal variations are possible (D. Li et al. 2021; S. B. Zhang et al. 2024). In addition, we use only the "gold" sample from CHIME/FRB Collaboration et al. (2023). The "silver" sample, which may be contaminated by chance coincidence, may yield CHIME repeating FRBs with a lower rate. As a result, this hardly totally excludes the possibility that FRB 20250316A would be detected in some distant future.

4.3. Constraints on Multiwavelength Counterparts

Different kinds of X-ray counterparts are expected for FRBs. Prompt X-ray pulses with durations ranging from milliseconds to seconds are anticipated in the magnetar framework. Such counterparts were detected in association with bright radio pulses from the Galactic magnetar SGR 1935+2154 (S. Mereghetti et al. 2020; C. K. Li et al. 2021; C. W. Wang et al. 2022). Our observations do not cover the time of FRB 20250316A itself, so we do not focus on this case in detail.

Persistent X-ray emission is also expected in various models. In the magnetar scenario, outbursts of persistent X-ray emission are usually observed during periods of enhanced bursting and flaring activity (V. M. Kaspi & A. M. Beloborodov 2017; F. Coti Zelati et al. 2018; N. Rea & D. De Grandis 2025), as in the case of the X-ray burst from the Galactic magnetar SGR 1935+2154 associated with FRB 20200428D (C. D. Bochenek et al. 2020; CHIME/FRB Collaboration et al. 2020). Typical long-term X-ray outbursts of magnetars might last several months to years, reaching a maximum luminosity of $\sim 10^{36}$ erg s^{-1} (V. M. Kaspi & A. M. Beloborodov 2017), where most of the luminosity is expected to be released in neutrinos (J. A. Pons & N. Rea 2012). Given our upper limit of $\sim 10^{39}$ erg s^{-1}, we cannot place meaningful constraints on such persistent magnetar outbursts. However, if FRBs are produced by a very young magnetar with fast rotation, one might expect a large amount of rotational power ($E_{\rm rot}$) that could support an X-ray counterpart in the form of pulsed synchrotron emission or a wind nebula. For example, by assuming (1) a magnetic field of at least $\sim 10^{14}$ G (required for the magnetar to show large X-bursts related to the FRB radio counterpart; R. Turolla et al. 2015) and (2) an X-ray efficiency of $\epsilon_{\rm X} \sim 10^{-3}$ (in line with rotationally powered young pulsars; A. Possenti et al. 2002), our deep upper limit implies a maximum rotational power for the young magnetar of $E_{\rm rot} < 10^{42}$ erg s^{-1} (assuming a neutron star mass of 1.4 $M_\odot$ and a radius of 12 km). Under these assumptions, the putative young magnetar responsible for FRB 20250316A would have a spin period larger than $P > 50$ ms and a characteristic age longer than 1 yr, possibly in line with the magnetar population of this star-forming galaxy.

Recent FRB environment studies and possible periodicities imply a possible link to binary systems (K. Ioka & B. Zhang 2020; F. Y. Wang et al. 2022; R. Anna-Thomas et al. 2023; Y. Li et al. 2025; B. Zhang & R.-C. Hu 2025). Thus, neutron star binary systems, especially LMXB, HMXBs, and ULXs, might also be related to FRBs.

In Figure 6, we compare the persistent X-ray luminosity upper limit of FRB 20250316A with those expected from different neutron star classes, both in isolation and in binary systems. We also overplot upper limits from other deep X-ray observations, including the repeating FRB 20200120E (gray open arrow; A. B. Pearlman et al. 2025), as well as the nonrepeating FRB 20200430A and FRB 20190608B (gray filled arrows; T. Eftekhari et al. 2023). The Chandra X-ray upper limit of FRB 20250316A is fainter than nearly all ULXs, while still compatible with an X-ray binary or a magnetar. It is deeper than previously reported limits for other nonrepeating FRBs but less constraining than the limit for the repeating FRB 20200120E. Although the strong variability observed in some ULXs prevents us from completely ruling out these systems as possible progenitors of FRB 20250316A, this result disfavors a direct connection between nonrepeating FRBs and ULXs, in agreement with previous findings for the repeating FRB 20200120E.

On the other hand, if FRBs are accompanied by outflows, multiwavelength afterglows are expected, typically lasting for days (S.-X. Yi et al. 2014). In the right panel of Figure 6, we present the X-ray upper-limit constraints obtained from EP-WXT, EP-FXT, and Chandra, together with the optical upper-

limit constraints from SVOM and WFST for FRB 20250316A. Here the 3σ values of EP J120944.2+585060 are adopted as upper limits of the FRB. Based on the X-ray upper-limit constraints and assuming that the source is viewed on-axis (which yields the strongest constraint on the kinetic energy), three possible scenarios can be considered:

1. *Ultrarelativistic outflow.* If the fireball decelerates before the first WXT observation (i.e., for $\Gamma \gtrsim 100$), the WXT point at $\sim$0.1 days provides the most stringent kinetic energy constraint, $E_k \lesssim 6 \times 10^{50}$ erg. The first FXT point at $\sim$1 day then limits the jet opening angle to $\sim 5^\circ$, requiring a jet break before $\sim$0.5 days to keep the X-ray flux below the FXT measurements (see blue solid line). The corresponding optical emission (orange solid line) is also consistent with the upper limits from SVOM and WFST, as well as the absence of radio counterparts (T. An et al. 2025).
2. *Moderately wide jet.* For a larger jet opening angle of $\theta_j \sim 17^\circ$, the jet break occurs near the first FXT observation. In this case, the WXT data no longer provide the strongest constraint. Instead, the first FXT point sets the dominant limit, yielding $E_k \lesssim 7 \times 10^{49}$ erg. The corresponding X-ray and optical light curves are shown by the blue and orange dashed lines, respectively.
3. *Low Lorentz factor outflow.* If the fireball decelerates around $\sim$1 day (near the FXT points), the inferred Lorentz factor is relatively low, $\Gamma \sim 5$. In this scenario, the FXT upper limits do not constrain the jet kinetic energy. Instead, the optical upper limits from SVOM and WFST dominate, requiring $E_k \lesssim 1.2 \times 10^{51}$ erg. The corresponding X-ray light curve is shown as the blue dotted line. If we take the MMT upper limit ($r > 25$ mag) and Gemini ($g > 23.7$ mag on 2025 March 24) into account, it requires $E_k \lesssim 8 \times 10^{50}$.

These kinetic energy constraints are far larger than the typical FRB energy budget. Therefore, if a hypothetical FRB afterglow exists, the required radio efficiency, $\sim E_{\rm FRB}/E_k$, would have to be $\gtrsim 10^{-12}$. It is obvious that an early deep X-ray observation is important to further constrain the X-ray counterpart predicted by the afterglow model.

5. Summary

In this paper, we present multiwavelength follow-up observations of the nearby bright apparent one-off FRB 20250316A, including radio observations with FAST, X-ray observations with EP and Chandra, and optical observations with WFST and SVOM/VT. The nondetection of pulses with the FAST radio telescope indicates that the predicted rate of well-studied repeating FRBs at the FAST limiting fluence is 2–8 orders of magnitude higher than FAST's 3σ upper limit and that the effective FRB rate at the CHIME limiting fluence is lower than the rates of all known repeating FRBs. These results suggest that this burst is distinct from the current sample of repeating FRBs and is likely a one-off event, supporting the results of CHIME/FRB Collaboration et al. (2025). The EP-WXT obtained the first upper limit of 7.2×10^{-12} erg cm^{-2} s^{-1} at just 3.5 hr post-burst, followed by the EP-FXT achieving a much deeper limit of 3.4×10^{-14} erg cm^{-2} s^{-1} at 1.4 days after the FRB. The subsequent Chandra observations established the most constraining 0.5–10 keV flux upper limit of 7.6×10^{-15} erg cm^{-2} s^{-1}, corresponding to an X-ray luminosity upper limit of $\sim 10^{39}$ erg s^{-1}, which is lower than those of most ULXs. These results place one of the most stringent limits on persistent X-ray emission from a nonrepeating FRB, disfavoring the association of FRBs with ULXs and providing critical constraints for theoretical models of FRB progenitors and emission processes. In addition, the combination of the optical and X-ray upper limits constrains the kinetic energy of afterglow models to $\lesssim 10^{51}$ erg.

Based on the chance coincidence probability estimation, we should be cautious about future FRB multiwavelength counterpart searches: arcsecond-level localization of both FRBs and their potential X-ray counterparts is essential for a convincing counterpart search.

Acknowledgments

This work is based on data from Einstein Probe, a space mission supported by the Strategic Priority Program on Space Science of the Chinese Academy of Sciences, in collaboration with the European Space Agency (ESA), the Max-Planck-Institute for Extraterrestrial Physics, and the Centre National d'Études Spatiales (CNES; grant No. XDA15310000 and XDB0550400). This research uses Chandra data sets from the Chandra X-ray Observatory DOI: 10.25574/cdc.480. FAST, a Chinese national mega-science facility, is built and operated by the National Astronomical Observatories, CAS. WFST is jointly operated by the University of Science and Technology of China and Purple Mountain Observatory. The Space Variable Objects Monitor (SVOM) is a joint Chinese–French mission led by the Chinese National Space Administration (CNSA), CNES, and CAS.

This work is supported by the Strategic Priority Research Program of the Chinese Academy of Sciences (grant No. XDB0550200), the National Natural Science Foundation of China (grant Nos. 12041306, 12321003, 12103089, 12393813, 12025303, 12041303, 12421003), the National Key Research and Development Program of China (2022SKA0130100, 2020SKA0120200), International Partnership Program of Chinese Academy of Sciences for Grand Challenges (114332KYSB20210018), the CAS Project for Young Scientists in Basic Research (grant No. YSBR-063), the CAS Organizational Scientific Research Platform for National Major Scientific and Technological Infrastructure: Cosmic Transients with FAST, the Young Elite Scientists Sponsorship Program by the China Association for Science and Technology (grant No. YESS20240218), and the Beijing Nova Program (No. 20250484786).

Appendix

Table A1 lists the optical observations and upper limits of each observation.

Table A1
Example of Optical Observations and Upper Limits

No	Telescope	Start Time	MJD	Filter	$\rm mag_{lim}$
1	WFST	2025-03-22 17:04:19	60756.71133	*r*	23.12

Note. Only the first few rows are shown here; the full table is available in the online version as a supplementary file.

(This table is available in its entirety in machine-readable form in the online article.)

ORCID iDs

Ye Li https://orcid.org/0000-0001-5931-2381
Hui Sun https://orcid.org/0000-0002-9615-1481
Lei Qian https://orcid.org/0000-0003-0597-0957
Dong-Yue Li https://orcid.org/0000-0002-4562-7179
Cheng-Kui Li https://orcid.org/0000-0001-5798-4491
Yi-Han Wang https://orcid.org/0000-0002-8614-8721
Tian-Rui Sun https://orcid.org/0000-0003-1166-3814
Jin-Jun Geng https://orcid.org/0000-0001-9648-7295
Nanda Rea https://orcid.org/0000-0003-2177-6388
Tao An https://orcid.org/0000-0003-4341-0029
Vadim Burwitz https://orcid.org/0000-0001-5330-5869
Yong Chen https://orcid.org/0000-0001-9834-2196
Hua-Qing Cheng https://orcid.org/0000-0003-4200-9954
Hua Feng https://orcid.org/0000-0001-7584-6236
Jing-Wei Hu https://orcid.org/0000-0002-0779-1947
Lei Hu https://orcid.org/0000-0001-7201-1938
Shu-Mei Jia https://orcid.org/0000-0002-5203-8321
Ji-An Jiang https://orcid.org/0000-0002-9092-0593
Yi-Fang Liang https://orcid.org/0009-0005-0170-192X
He-Yang Liu https://orcid.org/0000-0002-2412-5751
Arne Rau https://orcid.org/0000-0001-5990-6243
Xin-Wen Shu https://orcid.org/0000-0002-7020-4290
Lian Tao https://orcid.org/0000-0002-2705-4338
Jing Wang https://orcid.org/0000-0002-6880-4481
Yongquan Xue https://orcid.org/0000-0002-1935-8104
Xuan Yang https://orcid.org/0009-0009-3517-6640
Yuhan Yao https://orcid.org/0000-0001-6747-8509
Wen Zhao https://orcid.org/0000-0002-1330-2329
Jia-Heng Zhang https://orcid.org/0009-0009-3949-4726
Juan Zhang https://orcid.org/0000-0001-8869-0672
Song-Bo Zhang https://orcid.org/0000-0003-2366-219X
Yong-Kun Zhang https://orcid.org/0000-0002-8744-3546
Wei-Wei Zhu https://orcid.org/0000-0001-5105-4058
Peng Jiang https://orcid.org/0009-0003-3527-8520
Xue-Feng Wu https://orcid.org/0000-0002-6299-1263
Bing Zhang https://orcid.org/0000-0002-9725-2524

References

An, T., Wang, A., Huang, Y.-C., et al. 2025, arXiv:2508.05552
Andrew, S. & Chime/FRB Collaboration 2025, ATel, 17114, 1
Anna-Thomas, R., Connor, L., Dai, S., et al. 2023, Sci, 380, 599
Becker, A., 2015 HOTPANTS: High Order Transform of PSF ANd Template Subtraction-đ Astrophysics Source Code Library, ascl:1504.004
Bertin, E. 2006, in ASP Conf. Ser. 351, Astronomical Data Analysis Software and Systems XV, ed. C. Gabriel et al. (ASP), 112
Bertin, E., & Arnouts, S. 1996, A&AS, 117, 393
Bertin, E., Mellier, Y., Radovich, M., et al. 2002, in ASP Conf. Ser. 281, Astronomical Data Analysis Software and Systems XI, ed. D. A. Bohlender, D. Durand, & T. H. Handley (ASP), 228
Bhardwaj, M., Gaensler, B. M., Kaspi, V. M., et al. 2021, ApJL, 910, L18
Blanchard, P. K., Berger, E., Andrew, S. E., et al. 2025, ApJL, 989, L49
Bochenek, C. D., Ravi, V., Belov, K. V., et al. 2020, Natur, 587, 59
Chambers, K. C., et al. 2016, arXiv:1612.05560
Chen, Y., Cui, W., Han, D., et al. 2021, Proc. SPIE, 11444, 114445B
Chen, Y., Han, D., Cui, W., et al. 2025, Proc. SPIE, 13531, 1353102
Cheng, H., Zhang, C., Ling, Z., et al. 2025, ExA, 60, 15
CHIME/FRB Collaboration, Abbott, T. C., Amouyal, D., et al. 2025, ApJL, 989, L48
CHIME/FRB Collaboration, Amiri, M., Andersen, B. C., et al. 2020, Natur, 582, 351
CHIME/FRB Collaboration, Amiri, M., Andersen, B. C., et al. 2021, ApJS, 257, 59
CHIME/FRB Collaboration, Andersen, B. C., Bandura, K., et al. 2023, ApJ, 947, 83, 10.3847/1538-4357/acc6c1
CHIME/FRB Collaboration, Andersen, B. C., Bandura, K. M., et al. 2020, Natur, 587, 54
Cook, A. M., Scholz, P., Pearlman, A. B., et al. 2024, ApJ, 974, 170
Coti Zelati, F., Rea, N., Pons, J. A., Campana, S., & Esposito, P. 2018, MNRAS, 474, 961
Eftekhari, T., Fong, W., Gordon, A. C., et al. 2023, ApJ, 958, 66
Eppel, F., Krumpe, M., Limaye, P., et al. 2025, A&A, 695, L10
Feng, H., & Soria, R. 2011, NewAR, 55, 166
FRB Collaboration, Abbott, T. C., Amouyal, D., et al. 2025, ApJL, 989, L48
Fruscione, A., McDowell, J. C., Allen, G. E., et al. 2006, Proc. SPIE, 6270, 62701V
Gilfanov, M., Fabbiano, G., Lehmer, B., & Zezas, A. 2022, in Handbook of X-Ray and Gamma-Ray Astrophysics, ed. C. Bambi & A. Sangangelo (Springer), 105
Gourdji, K., Michilli, D., Spitler, L. G., et al. 2019, ApJL, 877, L19
Hewitt, D. M., Snelders, M. P., Hessels, J. W. T., et al. 2022, MNRAS, 515, 3577
Ioka, K., & Zhang, B. 2020, ApJL, 893, L26
Joseph, P., & Dagore, A. 2024, Astrometry.Net Index Files for Astrometry on UVIT Images, v1, Zenodo, doi:10.5281/zenodo.12684908
Kaaret, P., Feng, H., & Roberts, T. P. 2017, ARA&A, 55, 303
Kaspi, V. M., & Beloborodov, A. M. 2017, ARA&A, 55, 261
Kirsten, F., Marcote, B., Nimmo, K., et al. 2022, Natur, 602, 585
Kirsten, F., Ould-Boukattine, O. S., Herrmann, W., et al. 2024, NatAs, 8, 337
Kovlakas, K., Zezas, A., Andrews, J. J., et al. 2020, MNRAS, 498, 4790
Laha, S., Younes, G., Wadiasingh, Z., et al. 2022, ApJ, 930, 172
Lang, D., Hogg, D. W., Mierle, K., Blanton, M., & Roweis, S. 2010, AJ, 139, 1782
Law, C. J., Abruzzo, M. W., Bassa, C. G., et al. 2017, ApJ, 850, 76
Leung, C. & Chime/Frb Collaboration 2025, ATel, 17086, 1
Li, C. K., Lin, L., Xiong, S. L., et al. 2021, NatAs, 5, 378
Li, D., Wang, P., Zhu, W. W., et al. 2021, Natur, 598, 267
Li, T. P., & Ma, Y. Q. 1983, ApJ, 272, 317
Li, Y., Zhang, S. B., Yang, Y. P., et al. 2025, arXiv:2503.04727
Lorimer, D. R., Bailes, M., McLaughlin, M. A., Narkevic, D. J., & Crawford, F. 2007, Sci, 318, 777
Luo, R., Wang, B. J., Men, Y. P., et al. 2020, Natur, 586, 693
Masini, A., Hickox, R. C., Carroll, C. M., et al. 2020, ApJS, 251, 2
Mereghetti, S., Savchenko, V., Ferrigno, C., et al. 2020, ApJL, 898, L29
Mukai, K. 1993, Legacy, 3, 21
Ng, M. & CHIME/FRB Collaboration 2025, ATel, 17081, 1
Oostrum, L. C., Maan, Y., van Leeuwen, J., et al. 2020, A&A, 635, A61
Oppermann, N., Yu, H.-R., & Pen, U.-L. 2018, MNRAS, 475, 5109
Ould-Boukattine, O. S., Blaauw, R., Buchsteiner, T., et al. 2025, ATel, 17124, 1
Ould-Boukattine, O. S., Chawla, P., Hessels, J. W. T., et al. 2025, MNRAS, in press
Pearlman, A. B., Scholz, P., Bethapudi, S., et al. 2025, NatAs, 9, 111
Pilia, M., Burgay, M., Possenti, A., et al. 2020, ApJL, 896, L40
Pons, J. A., & Rea, N. 2012, ApJL, 750, L6
Possenti, A., Cerutti, R., Colpi, M., & Mereghetti, S. 2002, A&A, 387, 993
Principe, G., Di Venere, L., Negro, M., et al. 2023, A&A, 675, A99
Qian, L., Niu, J. R., Cao, J. H., et al. 2025, ATel, 17126, 1
Rajwade, K. M., Mickaliger, M. B., Stappers, B. W., et al. 2020, MNRAS, 495, 3551
Ransom, S. M. 2001, PhD thesis, Harvard University, Massachusetts
Ransom, S. M., Cordes, J. M., & Eikenberry, S. S. 2003, ApJ, 589, 911
Ransom, S. M., Eikenberry, S. S., & Middleditch, J. 2002, AJ, 124, 1788
Rea, N., & De Grandis, D. 2025, arXiv:2503.04442
Ridnaia, A., Frederiks, D., & Svinkin, D. 2024, MNRAS, 527, 5580
Robitaille, T., Deil, C., & Ginsburg, A., 2020 reproject: Python-based Astronomical Image Reprojection, Astrophysics Source Code Library, ascl:2011.023
Scholz, P., Cook, A., Cruces, M., et al. 2020, ApJ, 901, 165
Scholz, P., Spitler, L. G., Hessels, J. W. T., et al. 2016, ApJ, 833, 177
Sharma, K., Ravi, V., Connor, L., et al. 2024, Natur, 635, 61
Sorce, J. G., Tully, R. B., Courtois, H. M., et al. 2014, MNRAS, 444, 527
Spitler, L. G., Scholz, P., Hessels, J. W. T., et al. 2016, Natur, 531, 202
Sun, H., Cheng, H. Q., Li, D. Y., et al. 2025a, ATel, 17100, 1
Sun, H., Li, D. Y., Jin, C. C., et al. 2025b, ATel, 17119, 1
Swartz, D. A., Soria, R., Tennant, A. F., & Yukita, M. 2011, ApJ, 741, 49
Sydnor, J., Burke-Spolaor, S., Aggarwal, K., et al. 2025, ApJ, 984, 178
Tody, D. 1986, Proc. SPIE, 627, 733
Tody, D. 1993, ADASSII, 52, 173
Tully, R. B., Courtois, H. M., & Sorce, J. G. 2016, AJ, 152, 50

Turolla, R., Zane, S., & Watts, A. L. 2015, RPPh, 78, 116901
Verrecchia, F., Casentini, C., Tavani, M., et al. 2021, ApJ, 915, 102
Wang, C. W., Xiong, S. L., Zhang, Y. Q., et al. 2022, ATel, 15682, 1
Wang, F. Y., Zhang, G. Q., Dai, Z. G., & Cheng, K. S. 2022, NatCo, 13, 4382
Wang, S., Qiu, Y., Liu, J., & Bregman, J. N. 2016, ApJ, 829, 20
Wang, T., Liu, G., Cai, Z., et al. 2023, SCPMA, 66, 109512
Wang, Y., Chen, C., & Zhang, B. 2026, JHEAp, 50, 100490
Waratkar, G., Dixit, M., Tendulkar, S. P., et al. 2025, JApA, 46, 59
Wei, J., Cordier, B., Antier, S., et al. 2016, arXiv:1610.06892
Yi, S.-X., Gao, H., & Zhang, B. 2014, ApJL, 792, L21
Yuan, W., Zhang, C., Chen, Y., & Ling, Z. 2022, in Handbook of X-ray and Gamma-ray Astrophysics, ed. C. Bambi & A. Sangangelo (Springer), 86
Zhang, B. 2024, ARNPS, 74, 89
Zhang, B., & Hu, R.-C. 2025, arXiv:2508.12119
Zhang, S. B., Wang, J. S., Yang, X., et al. 2024, NatCo, 15, 7454
Zhang, Y.-K., Wang, P., Feng, Y., et al. 2022, RAA, 22, 124002